New MIC Power Dividers Using Coupled Microstrip-Slot Lines: Two-Sided MIC Power Dividers

HIROYO OGAWA, MEMBER, IEEE, TETSUO HIROTA, AND MASAYOSHI AIKAWA, MEMBER, IEEE

Abstract —New microwave integrated circuit (MIC) power dividers have been proposed. These power dividers utilize both substrate surfaces and employ coupled microstrip-slot lines,[1] microstrip lines, and slotlines; therefore, we make use of the two-sided MIC[2] technique. The out-of-phase-type power dividers, as well as the in-phase-type circuits, can be constructed by the circuit configuration method described in this paper. Coupled microstrip-slot lines, an important component of the power dividers, have been analyzed by the spectral-domain method, and their characteristics have been calculated and the numerical results shown for several different structural parameters for the purpose of designing power dividers. The out-of-phase-type power divider was fabricated at the 26-GHz band and good performance achieved, confirming the calculated accuracy through experimental results. The new two-sided MIC power dividers are expected to have wide applications at the millimeter-wave band.

I. Introduction

RECENTLY, microwave integrated circuits (MIC's) have been generally used to produce various circuits [1], [2]. Transmitters and receivers have also been fabricated by combinations of these components [3]–[5]. Microstrip lines are mainly used as transmission lines and constructed only on the one side of the substrate. Accordingly, high-performance balanced-type circuits with simple configuration and low circuit loss are not easily realized at high-frequency bands over the quasi-millimeter-wave band, because the microstrip line has the following shortcomings.

1) The attainable upper limit of the characteristic impedance is considerably smaller than that of the slotline.

2) Series splitting circuits cannot be obtained by the simple configuration.

3) Microstrip line couplers with a tight coupling coefficient cannot be realized because of a restrictive manufacturing process (except the Lange coupler).

4) The extent of the producible circuit configuration is limited because the microstrip line circuit uses only one substrate surface.

In order to overcome these problems, two-sided MIC's consisting of combinations of microstrip lines, slotlines, and coplanar lines have been proposed. These effectively utilize both substrate surfaces and realize such high-performance circuits at high-frequency bands as magic-T [6], [7], 3-dB directional coupler [8], [9], double-balanced mixer [10], image-enhanced mixer [11], and balanced phase-shift keying (PSK) modulator [12], [13]. However, two-sided MIC power dividers with three input/output ports and constructed with coupled microstrip slotlines have as yet not been reported or fabricated, so far as the authors know [27]. Three-port power dividers are passive circuits useful in producing PSK modulators and high-power amplifiers [14].

In this paper, new configurations of power dividers are proposed. They consist of quarter-wavelength coupled microstrip-slot lines, a thin-film resistor, and input/output microstrip lines or slotlines. They can produce various two-sided MIC's with many functions and high performance at high-frequency bands.

First, the circuit configurations of two-sided MIC power dividers are described. Second, the equivalent circuit of the power divider is shown and the design formulas are presented, and then the performance limitation of the power divider composed of coupled lines is evaluated. Third, the spectral-domain analysis of the coupled microstrip slotlines is reviewed briefly, and the numerical results are given and compared with other available data. Finally, the experimental results at the 26-GHz band are described.

II. Circuit Configuration

Power dividers are divided into two types, the in-phase dividing types and the out-of-phase ones. The former types are made of microstrip lines or coaxial lines [15], [16], while in the latter case, slotlines are used [17]. Since these circuits are composed of one transmission line, transition circuits are necessary to connect another circuit using a different kind of transmission line. This increases both circuit size and transmission loss.

Fig. 1 shows the circuit configuration of the new power dividers proposed in this paper. They are classified into two types, the out-of-phase type (Fig. 1(a) and (b)) and the in-phase type (Fig. 1(c) and (d)), according to the kind of input transmission line connected to their coupled microstrip slotlines. In this figure, the solid lines indicate microstrip lines on the substrate, while the dotted lines indicate slotlines on the reverse side of the substrate. The difference

Manuscript received February 11, 1985; revised June 21, 1985.

The authors are with the Yokosuka Electrical Communication Laboratory, Nippon Telegraph and Telephone Public Corporation, Yokosuka, 238 Japan.

[1]Since the combination of the microstrip line and the slotline can realize the distributed-type coupler [9], let us call it the coupled microstrip-slot lines.

[2]Since the circuit utilizes both substrate surfaces, let us call it the two-sided MIC [13].

0018-9480/85/1100-1155$01.00 ©1985 IEEE

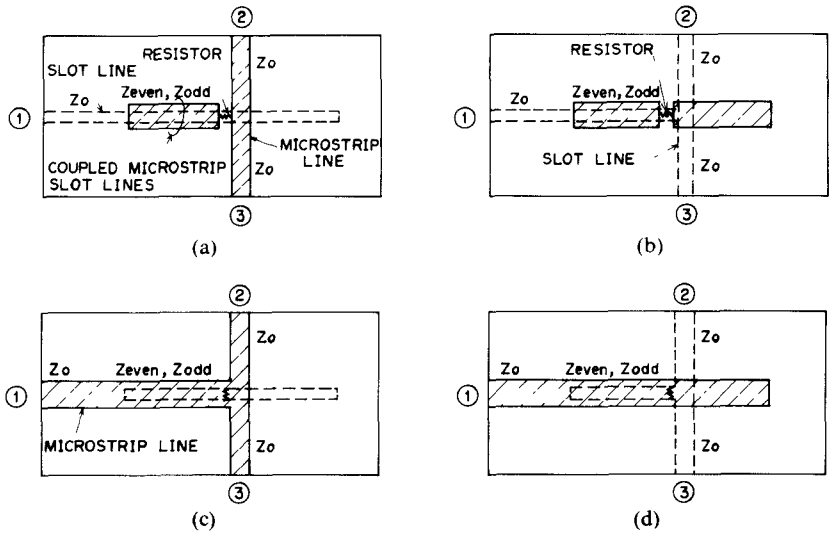

Fig. 1. Circuit configurations of two-sided MIC power dividers. Solid lines show microstrip lines on the substrate, dotted lines show slotlines on the reverse side of the substrate. (a) and (b) are the out-of-phase-type power dividers. (c) and (d) are the in-phase-type power dividers.

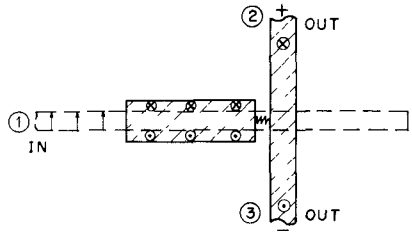

Fig. 2. Schematic fundamental behavior of power divider. Arrows represent the direction of electric field.

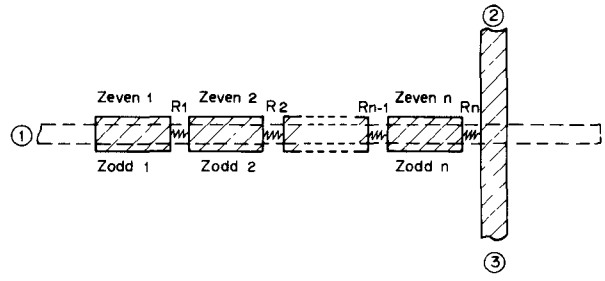

Fig. 3. Multisection out-of-phase-type power divider.

between Fig. 1(a) and (b) is the output transmission line. The out-of-phase output power is obtained from microstrip lines in Fig. 1(a), and from slotlines in Fig. 1(b). In Fig. 1(c) and (d), the in-phase output power comes from microstrip lines and slotlines, respectively. Therefore, the proposed power dividers composed of coupled microstrip-slot lines can be applied to various types of circuit configurations.

Fundamental behavior can be understood by examining the out-of-phase-type circuit in Fig. 1(a), because the behavior of the other types are the same in principle. Fig. 2 gives a schematic explanation of the circuit behavior. In this figure, arrows and circles containing a dot or $\times$ represent the schematic expression of the electric field in the slotline, the microstrip line, and the coupled microstrip-slot lines. The input signal fed to port 1 propagates through the slotline, and is then converted to the even mode of the coupled microstrip-slot lines. After propagation through the coupled lines, it is divided in an out-of-phase condition into two microstrip line ports (ports 2 and 3).

On the other hand, the in-phase-type circuits utilize the odd mode of the coupled microstrip-slot lines, because the input signal is incident on the microstrip line, which is followed by the coupled lines. The quarter-wavelength short-circuited slotlines and open-circuited microstrip lines in Fig. 1 assist in the efficient transition from the coupled microstrip-slot lines to the microstrip line or the slotline. The even- and odd-mode dispersion characteristics of the coupled microstrip-slot lines will be discussed in detail in a later section.

III. Design of the Power Divider

A. Design Formulas

Fig. 3 shows the multisection out-of-phase-type power divider which generalizes the circuit of Fig. 1(a). The design formulas have been derived for the out-of-phase-type circuit, but these equations can also be adapted for designing the in-phase-type by exchanging the even-mode characteristic impedance (Z_{even}) for the odd-mode one (Z_{odd}). The multisection technique is used to increase the bandwidth of the power divider [18].

The symmetrical circuit in Fig. 3 is analyzed by a method employing in-phase and out-of-phase excitation of ports 2 and 3 with a load impedance of Z_0 connected to port 1 [19]. Fig. 4 shows the two equivalent circuits which are obtained when ports 2 and 3 are excited by the out-of-phase and in-phase signals. In this figure, θ_{even} and θ_{odd} are the electrical length of the even mode and the odd mode of the coupled microstrip slotlines, respectively.

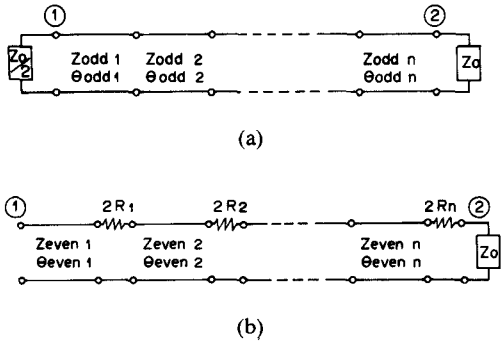

Fig. 4. Equivalent circuits for the out-of-phase and the in-phase excitations. (a) Out-of-phase excited circuit. (b) In-phase-excited circuit.

Let ρ_o and ρ_e be the voltage reflection coefficients of the circuits in Fig. 4(a) and (b). The voltage reflection coefficient ρ_1, ρ_2, and ρ_3 at ports 1, 2 and 3, and the voltage transmission coefficient t_{12}, t_{13}, and t_{23} between these ports are expressed as follows [18], [19]:

$$\rho_1 = \rho_o \tag{1}$$

$$t_{12} = t_{13};\ |t_{12}| = |t_{13}| = \frac{1}{\sqrt{2}}\left(1-\rho_o^2\right)^{1/2} \tag{2}$$

$$\rho_2 = \rho_3 = \frac{1}{2}(\rho_o + \rho_e) \tag{3}$$

$$t_{23} = \frac{1}{2}(\rho_o - \rho_e). \tag{4}$$

All characteristics of the circuit in Fig. 3 are calculated by the above equations; however, the even- and odd-mode characteristic impedances and the resistances still remain unknown parameters.

By adapting Cohn's results and considering the following conditions, these parameters can be determined. The restricted conditions are as follows.

1) The odd-mode characteristic impedances $Z_{\mathrm{odd}i}$ $(i=1 \sim n)$ are designed to yield optimum stepped-transformer response between terminal impedance Z_0 and $Z_0/2$. Optimum performance means equal-ripple behavior in a specified bandwidth between f_1 and f_2. The electrical lengths $\theta_{\mathrm{odd}i}$ $(i=1 \sim n)$ are equal to 90°.

2) The resistances R_i $(i=1 \sim n)$ are calculated from the impedance-matching condition of port 2 in Fig. 4(b). The even-mode electrical lengths $\theta_{\mathrm{even}i}$ $(i=1 \sim n)$ are also equal to 90°.

The design formulas are derived up to the three-section power divider. All characteristic impedances and resistances are normalized by the load impedance of Z_0.

One-Section Power Divider:

$$Z_{\mathrm{odd}1} = \frac{1}{\sqrt{2}} \tag{5}$$

$$R_1 = \frac{1}{2}. \tag{6}$$

Two-Section Power Divider:

$$Z_{\mathrm{odd}1} = \frac{A}{2} \tag{7}$$

$$Z_{\mathrm{odd}2} = \frac{1}{A} \tag{8}$$

$$R_1 = \frac{1}{4}\left(\frac{1}{Z_{\mathrm{even}1}^2} - \frac{\cot^2\theta}{Z_{\mathrm{even}2}^2} - 2\cot^2\theta + 2\right)^{1/2} \tag{9}$$

$$R_2 = \frac{Z_{\mathrm{even}1} + Z_{\mathrm{even}2} - 2R_1 Z_{\mathrm{even}2}}{2(Z_{\mathrm{even}1} + Z_{\mathrm{even}2})} \tag{10}$$

where

$$A = \left\{\left(2 + \frac{1}{4\tan^4\theta}\right)^{1/2} + \frac{1}{2\tan^2\theta}\right\}^{1/2} \tag{11}$$

$$\cos^2\theta = \frac{1}{2}\cos^2\frac{\pi}{1+f_2/f_1}. \tag{12}$$

Three-Section Power Divider:

$Z_{\mathrm{odd}1}$ is the positive real number which satisfies the following fourth-order equation:

$$8Z_{\mathrm{odd}1}^4 + 8\sqrt{2}\,Z_{\mathrm{odd}1}^3 - \frac{2}{\tan^2\theta}Z_{\mathrm{odd}1}^2 - 2\sqrt{2}\,Z_{\mathrm{odd}1} - 1 = 0 \tag{13}$$

$$Z_{\mathrm{odd}2} = \frac{1}{\sqrt{2}} \tag{14}$$

$$Z_{\mathrm{odd}3} = \frac{1}{2Z_{\mathrm{odd}1}} \tag{15}$$

$$R_1 = \left\{(Z_{\mathrm{even}1} + Z_{\mathrm{even}2})x\left(x + Z_{\mathrm{even}2}^2\right)\right\}^{1/2}/2B \tag{16}$$

$$R_2 = \frac{\sqrt{x}}{2}B\left\{(Z_{\mathrm{even}1} + Z_{\mathrm{even}2})\left(x + Z_{\mathrm{even}2}^2\right)\right\}^{1/2} \tag{17}$$

$$R_3 = \frac{1}{2}\left\{1 - Z_{\mathrm{even}3}^2\frac{\sqrt{(Z_{\mathrm{even}1} + Z_{\mathrm{even}2})x}}{\sqrt{x + Z_{\mathrm{even}2}^2 \cdot B}}\right\} \tag{18}$$

where

$$B = \left(Z_{\mathrm{even}1}Z_{\mathrm{even}2}Z_{\mathrm{even}3} + Z_{\mathrm{even}2}Z_{\mathrm{even}3}^2 + Z_{\mathrm{even}1}Z_{\mathrm{even}3}^2 - Z_{\mathrm{even}2}^3 - Z_{\mathrm{even}2}x\right)^{1/2} \tag{19}$$

$$\cos^2\theta = \frac{3}{4}\cos^2\frac{\pi}{1+f_2/f_1}. \tag{20}$$

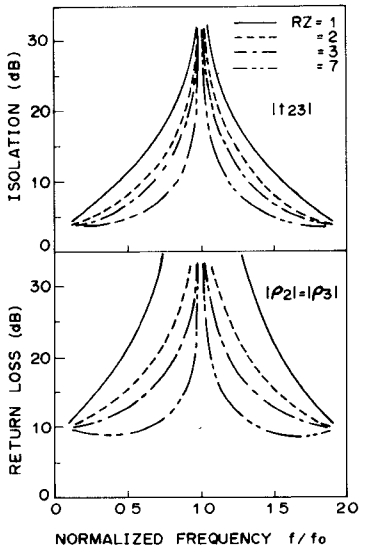

Fig. 5. Theoretical performance of power divider. $|t_{23}|$ represents the isolation between ports 2 and 3. $|\rho_2|$ and $|\rho_3|$ represent the return loss of ports 2 and 3, respectively. RZ shows the ratio of the even- and odd-mode characteristic impedances.

x is the positive real number of the next third-order equation.

$$x^3 + \alpha x^2 + \beta x + \gamma = 0 \tag{21}$$

$$\alpha = Z_{\text{even}2}\left(-\cot^2\theta \cdot Z_{\text{even}1} + 3Z_{\text{even}2} + Z_{\text{even}3}\right)$$

$$\begin{aligned}\beta = -\{&2Z_{\text{even}1}Z_{\text{even}2}^3 - Z_{\text{even}1}Z_{\text{even}3}(Z_{\text{even}1}Z_{\text{even}2} \\ &+ Z_{\text{even}2}Z_{\text{even}3} + Z_{\text{even}3}Z_{\text{even}1})\}\cdot\cot^2\theta + 2Z_{\text{even}2}^3Z_{\text{even}3} \\ &+ 3Z_{\text{even}2}^4 - Z_{\text{even}2}^2Z_{\text{even}3}^2 - Z_{\text{even}1}Z_{\text{even}2}Z_{\text{even}3}^2\end{aligned}$$

$$\begin{aligned}\gamma = -&\left(Z_{\text{even}1}Z_{\text{even}2}^5 - Z_{\text{even}1}^2Z_{\text{even}2}^3Z_{\text{even}3}\right. \\ &- Z_{\text{even}1}Z_{\text{even}2}^3Z_{\text{even}3}^2 - Z_{\text{even}1}^2Z_{\text{even}2}^2Z_{\text{even}3}^2)\cdot\cot^2\theta \\ &- 2Z_{\text{even}1}Z_{\text{even}2}^3Z_{\text{even}3}^2 - 2Z_{\text{even}1}Z_{\text{even}2}^2Z_{\text{even}3}^3 \\ &- Z_{\text{even}2}^3Z_{\text{even}3}^3 + Z_{\text{even}2}^5Z_{\text{even}3} - Z_{\text{even}1}^2Z_{\text{even}2}^2Z_{\text{even}3}^2 \\ &- Z_{\text{even}1}^2Z_{\text{even}2}Z_{\text{even}3}^3 - Z_{\text{even}2}^4Z_{\text{even}3}^2 + Z_{\text{even}2}^6.\end{aligned}$$

B. Theoretical Performance

As a calculation example of the power-divider performance, the one-section circuit characteristics are computed by using (3)–(6). Fig. 5 shows the isolation between ports 2 and 3, and the return loss at ports 2 and 3. The ratio of the even- and the odd-mode characteristic impedances ($RZ = Z_{\text{even}}/Z_{\text{odd}}$) is chosen as the parameter in this calculation, because these impedances have different values according to the width and gaps of the coupled microstrip slotlines, as will be shown in the next section.

When RZ is equal to 1.0, i.e., $Z_{\text{even}} = Z_{\text{odd}}$, the power divider is composed of noncoupled lines. This is the widest obtainable bandwidth of the one-section power divider. However, the larger the value of RZ, the more narrow the bandwidth obtained. This necessitates coupled microstrip slotlines with a slight difference between Z_{even} and Z_{odd}.

The reflection characteristic at port 1 and the transmission characteristics from port 1 to ports 2 or 3 are not deteriorated by the coupling because these coefficients are determined from out-of-phase excitation.

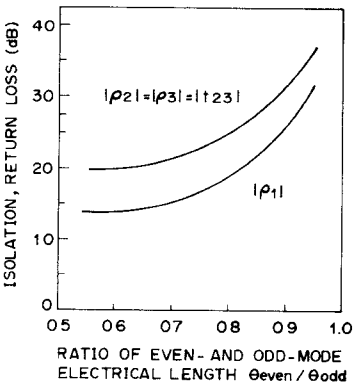

Fig. 6. Performance deterioration of power divider by means of the difference between the even- and odd-mode electrical lengths. $|\rho_1|$ represents the return loss of port 1.

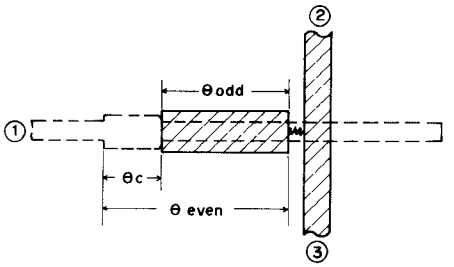

Fig. 7. Circuit configuration using a compensation circuit for the phase velocity difference.

In the above-mentioned discussion, the electrical length of the even mode is equal to that of the odd mode. Coupled lines generally have different phase velocities between the two orthogonal modes. Fig. 6 shows the isolation and the return loss degradation at the center frequency ($\theta_{\text{even}} = 90°$). The impedance ratio of RZ is equal to 4.0. Since the even-mode electrical length is fixed at 90°, the return loss at ports 2 and 3 is consistent to the isolation between ports 2 and 3.

This degradation problem can be solved by the compensation of the electrical length deviation between θ_{even} and θ_{odd}. Fig. 7 shows a circuit example of this compensation method. A slotline which has the characteristic impedance of $2Z_{\text{odd}}$ and the electrical length of $\theta_c = \theta_{\text{even}} - \theta_{\text{odd}}$ is connected to the coupled microstrip slotlines. This concept can also be employed in multisection power dividers. This is because the resistances have finite physical length and this portion of the slotline is designed to have a characteristic impedance of $2Z_{\text{odd}}$, making it possible for the phase velocity difference to be compensated at each section.

IV. Characteristics of Coupled Microstrip-Slot Lines

In designing a power divider, the two orthogonal-mode characteristics of the coupled microstrip-slot lines must be evaluated. Fig. 8 shows the schematic expression of the even- and odd-mode electric fields [20]. The spectral-domain analysis proposed by Itoh and Mittra is adopted to calculate the propagation constant and the characteristic impedance of each mode because of its simplicity and

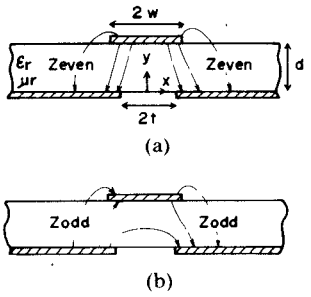

Fig. 8. Schematic expressions for the even- and odd-mode electric fields of coupled microstrip-slot lines. (a) Even mode. (b) Odd mode.

extreme accuracy [21], [22]. In this section, an outline of an analysis of the coupled microstrip-slot lines is described and numerical results are given for several different structural parameters.

A. Application of Spectral-Domain Analysis

It is assumed that the coupled microstrip-slot lines in Fig. 8 are composed of perfect conductors, and that the substrate material is lossless, and has a relative permittivity and permeability of ϵ_r and μ_r, respectively. All hybrid-field components can be obtained from a superposition of TE and TM modes which are related to the scalar potentials $\psi^{(e)}(x, y)$ and $\psi^{(h)}(x, y)$, where the superscripts e and h denote electric and magnetic, respectively. These scalar potential functions satisfy the Helmholtz equation. The solutions are obtained in the Fourier transformed domain. The Fourier transforms of the scalar functions are defined as follows:

$$\tilde{\psi}_i^{(p)}(\alpha, y) = \int_{-\infty}^{\infty} \psi_i^{(p)}(x, y) e^{j\alpha x} \alpha x, \qquad i = 1,2,3,\ p = e \text{ or } h \quad (22)$$

The solutions for the regions 1, 2, and 3 are written as

$$\begin{aligned}
\tilde{\psi}_1^{(e)}(\alpha, y) &= A^{(e)}(\alpha) \exp\left[-\gamma_1(y-d)\right] \\
\tilde{\psi}_2^{(e)}(\alpha, y) &= B^{(e)}(\alpha) \sinh\gamma_2 y + C^{(e)}(\alpha) \cosh\gamma_2 y \\
\tilde{\psi}_3^{(e)}(\alpha, y) &= D^{(e)}(\alpha) \exp\left[\gamma_3 y\right] \\
\tilde{\psi}_1^{(h)}(\alpha, y) &= A^{(h)}(\alpha) \exp\left[-\gamma_1(y-d)\right] \\
\tilde{\psi}_2^{(h)}(\alpha, y) &= B^{(h)}(\alpha) \sinh\gamma_2 y + C^{(h)}(\alpha) \cosh\gamma_2 y \\
\tilde{\psi}_3^{(h)}(\alpha, y) &= D^{(h)}(\alpha) \exp\left[\gamma_3 y\right] \qquad (23)
\end{aligned}$$

where

$$\gamma_i^2 = \alpha^2 + \beta^2 - k_i^2 \quad k_1 = k_3 = k_0 \quad k_2 = \sqrt{\epsilon_r} k_0.$$

β is the unknown propagation constant and k_0 is the free-space wavenumber. The eight unknown coefficients $A^{(e)}(\alpha)$ through $D^{(h)}(\alpha)$ are obtained from the boundary and continuity conditions at the interfaces $y = 0$ and $y = d$. These coefficients are the functions of the Fourier transformed surface current density on the microstrip line ($\tilde{J}_x(\alpha)$, $\tilde{J}_z(\alpha)$) and the horizontal electric field components on the slotline ($\tilde{E}_x(\alpha)$, $\tilde{E}_z(\alpha)$). The exact expressions of $A^{(e)}(\alpha)$ through $D^{(h)}(\alpha)$ are shown in the Appendix.

The Fourier transforms of the x- and z-directed current-density and electric-field components on the surfaces $y = 0$ and $y = d$ are coupled through the following equations:

$$\begin{bmatrix} G_{11}(\alpha,\beta) & G_{12}(\alpha,\beta) & G_{13}(\alpha,\beta) & G_{14}(\alpha,\beta) \\ G_{21}(\alpha,\beta) & -G_{11}(\alpha,\beta) & G_{23}(\alpha,\beta) & G_{13}(\alpha,\beta) \\ G_{23}(\alpha,\beta) & -G_{13}(\alpha,\beta) & G_{33}(\alpha,\beta) & G_{34}(\alpha,\beta) \\ -G_{13}(\alpha,\beta) & G_{14}(\alpha,\beta) & G_{34}(\alpha,\beta) & G_{44}(\alpha,\beta) \end{bmatrix} \cdot \begin{bmatrix} \tilde{J}_x(\alpha) \\ -\tilde{J}_z(\alpha) \\ \tilde{E}_x(\alpha) \\ \tilde{E}_z(\alpha) \end{bmatrix} = \begin{bmatrix} \tilde{e}_z(\alpha) \\ \tilde{e}_x(\alpha) \\ \tilde{I}_x(\alpha) \\ \tilde{I}_z(\alpha) \end{bmatrix} \quad (24)$$

where the elements of the G matrix are the Fourier transforms of the dyadic Green's function components in the space domain and the closed-form functions of α and β. The exact formulas for Green's functions are given in the Appendix. In (24), $\tilde{e}_x(\alpha)$ and $\tilde{e}_z(\alpha)$ are the Fourier transforms of the horizontal electric field on dielectric material ($y = d$). $\tilde{I}_x(\alpha)$ and $\tilde{I}_z(\alpha)$ are the Fourier transforms of the current density on the ground conductor ($y = 0$).

In order to solve the algebraic equations given in (24), Galerkin's procedure is applied in the Fourier transform domain, and the electric-field and current-density components are expanded in terms of known basis functions. Equation (24) becomes the simultaneous equations. The propagation constant β can be obtained by setting the determinant of the coefficient matrix of equations equal to zero.

The characteristic impedances of the two orthogonal modes are calculated by the ratio of the average power flow traveling in the $+z$ direction (P_{av}) and the amplitude of the voltage across the slot (V_0) or the z-directed microstrip current (I_0) [23], [24]. The definition of the characteristic impedance for the even and odd modes is as follows:

$$Z_{even} = \frac{4P_{av}}{I_0^2} \quad (25)$$

$$Z_{odd} = \frac{V_0^2}{4P_{av}}. \quad (26)$$

The characteristic impedances of the microstrip line and the slotline are applied to the even- and odd-mode characteristic impedances, respectively, because the electric-field distribution of the microstrip line is similar to that of the even mode and the slotline to that of the odd mode, as shown in Fig. 8. The average power is calculated from the following equation:

$$P_{av} = \frac{1}{4\pi} R_e \int_{-\infty}^{\infty} g(\alpha)\, d\alpha \quad (27)$$

where

$$g(\alpha) = g_1(\alpha) + g_2(\alpha) + g_3(\alpha).$$

The function $g(\alpha)$ is obtained from the scalar potential

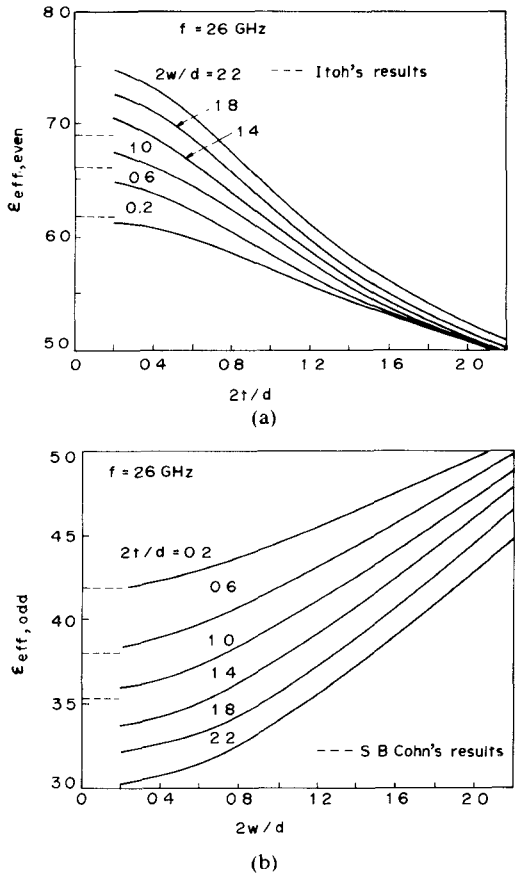

Fig. 9. Effective dielectric constants for the even and odd modes of coupled microstrip-slot lines on an alumina substrate. (a) Even mode. (b) Odd mode.

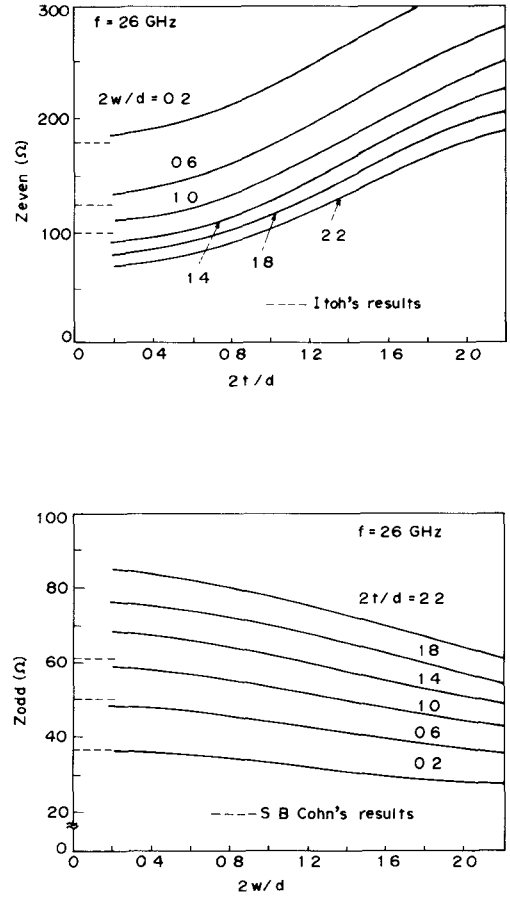

Fig. 10. Characteristic impedances for the even and odd modes of coupled microstrip-slot lines on an alumina substrate. (a) Even mode. (b) Odd mode.

functions. The numerical expressions of $g(\alpha)$ for each region are written in the Appendix.

B. Numerical Results

The following basis functions are chosen to determine the propagation constants and the characteristic impedances of the two orthogonal modes because of the highly accurate numerical results and short computation time which can be achieved [22], [24], [25].

For the Even Mode:

$$J_{z1}(x) = \begin{cases} 1, & |x| < w \\ 0, & |x| > w \end{cases}$$

$$E_{x1}(x) = \begin{cases} 1, & 0 < x < t \\ -1, & -t < x < 0 \\ 0, & |x| > t \end{cases}$$

$$E_{z1}(x) = \begin{cases} 1, & |x| < t \\ 0, & |x| > t \end{cases}. \tag{28}$$

For the Odd Mode:

$$E_{x1}(x) = \begin{cases} 1, & |x| < t \\ 0, & |x| > t \end{cases}$$

$$J_{x1}(x) = \begin{cases} 1, & |x| < w \\ 0, & |x| > w \end{cases}$$

$$J_{z1}(x) = \begin{cases} 1, & 0 < x < w \\ -1, & -w < x < 0. \\ 0, & |x| > w \end{cases} \tag{29}$$

Figs. 9 and 10 show the effective dielectric constants and the characteristic impedances of the two orthogonal modes. The relative permittivity ϵ_r and permeability μ_r of the substrate material are 9.6 and 1.0, respectively. A substrate thickness of 0.3 mm was chosen to accommodate the fabrication of a power divider on it. The dotted lines represent other available data calculated by Itoh's (for the even mode) and Cohn's (for the odd mode) methods. These data correspond to the effective dielectric constants and the characteristic impedances of the single microstrip line ($2t/d = 0$) and slotline ($2w/d = 0$). The good agreement between this and the method being presented was obtained. The average computation time for the effective dielectric constant and characteristic impedance using the DIPS-123-30 computer was 70 s for one given dimension.

V. Experimental Results

In order to confirm the fundamental behavior at high-frequency bands of the power divider, a one-section out-of-phase-type circuit was designed using the formulas described in the previous section at the center frequency of 26 GHz. Since the load impedance Z_0 is 50 Ω, Z_{odd1} is equal to 34.5 Ω (eq. (5)) and R_1 is equal to 25 Ω (eq. (6)). The dimensions of the coupled microstrip slotlines are determined from Fig. 9 so as to prevent isolation and return

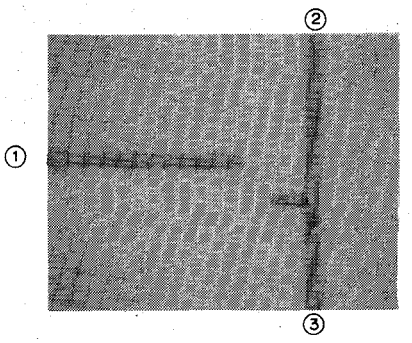

(a)

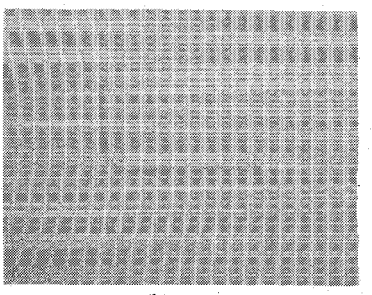

(b)

Fig. 11. Photographs of power divider. (a) Microstrip line pattern on the substrate. (b) Slotline pattern on the reverse surface.

loss degradation resulting from the difference between Z_{even} and Z_{odd}. Since the ratio of the electrical length θ_{even} and θ_{odd} can be set to a value of more than 0.8, and (as can be seen from Fig. 6) an isolation and the return loss of greater than 20 dB are achieved by that value, the arithmetic mean length of the two orthogonal modes is used as a quarter wavelength of the coupled microstrip slotlines.

The one-section power divider has been fabricated by the usual photolithographic technique on a 0.3-mm-thick alumina substrate with a relative permittivity of 9.6. Since the power divider requires a thin-film resistor, tantalum nitride (Ta_2N) is sputtered on the substrate. Then, nickel-chromium with a 500-Å thickness and gold with a 6000-Å thickness are deposited by the vacuum evaporation method. Thus, the construction of the metal layers on the substrate is a three-layer metal system, i.e., Ta_2N-NiCr-Au, while that on the reverse side of the substrate is a two-layer metal system, i.e., NiCr-Au. The thickness of the gold on the microstrip lines and slotlines is increased to about 4 μm by electroplating. The sheet resistance of the tantalum nitride is 35 Ω/square.

Fig. 11 shows photographs of the power-divider pattern. The patterns of the microstrip lines on the substrate and the slotlines on the reverse side are shown in Fig. 11(a) and (b), respectively. In this experiment, the ridged waveguide [26] is used to construct the waveguide-to-microstrip transition [28]. These transitions are connected to ports 1, 2, and 3.

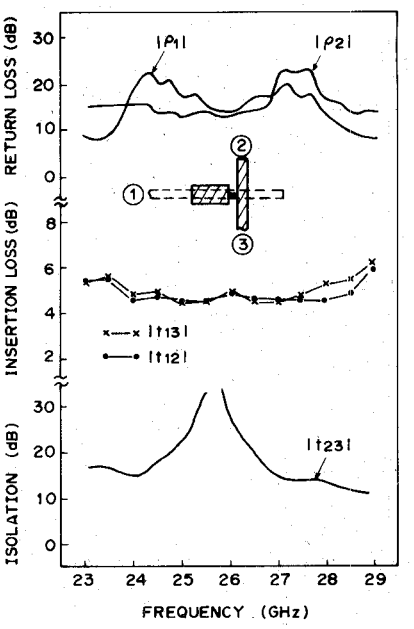

Fig. 12. Experimental performance of the power divider with a center frequency of 26 GHz.

The experimental data are shown in Fig. 12. The insertion loss ($|t_{12}|$, $|t_{13}|$) between ports 1 and 2 (or 3) is less than 5 dB for a frequency range of 24–27.5 GHz. The excess insertion loss is the mismatch loss at the connection point between the slotline and coupled microstrip slotlines, and the transition loss from the microstrip line connected at port 1 to the slotline. The insertion loss deviation between $|t_{12}|$ and $|t_{13}|$ is less than 0.5 dB over a range of 23–28 GHz. The isolation between ports 2 and 3 is greater than 20 dB over a bandwidth of 1.5 GHz. As a result, the fundamental behavior of the power divider using coupled microstrip slotlines has been confirmed by measurements at the 26-GHz band, and an out-of-phase-type power divider with good performance and simple configuration has been achieved by the two-sided MIC; that is, the combination of microstrip lines and slotlines on both substrate surfaces.

VI. Conclusion

New MIC power dividers have been proposed and successfully fabricated at the 26-GHz band. These power dividers utilize both substrate surfaces and employ coupled microstrip-slot lines, microstrip lines, and slotlines. Out-of-phase-type circuits, as well as in-phase ones, can be constructed through a two-sided MIC technique, particularly one employing coupled microstrip-slot lines.

The design formulas, the performance analysis, and the experimental results of the power divider have been described. According to the design expressions, an out-of-phase-type power divider was fabricated on an alumina substrate and its fundamental behavior was confirmed at the 26-GHz band.

In addition to these theoretical and experimental circuit investigations on the power divider, this paper described the analytical method for coupled microstrip-slot lines.

Numerical results for several different structural parameters are shown and compared with previous reported data. Good agreement between these data was obtained, and the calculated accuracy was also confirmed by measurements made on the power divider.

The power dividers proposed in this paper are expected to have wide applications at the millimeter-wave band. These circuits are useful in constructing such two-sided MIC's as balanced QPSK modulators and phase shifters. These power dividers will enable a greater variety of realizable MIC configurations.

Appendix

The exact expressions of unknown coefficients $A^{(e)}(\alpha)$ through $D^{(h)}(\alpha)$ of scalar functions $\tilde{\psi}_1^{(e)}(\alpha, y) \sim \tilde{\psi}_3^{(h)}(\alpha, y)$ are as follows:

$$A^{(e)}(\alpha) = \frac{\beta\omega\mu_1}{k_1^2-\beta^2}\sinh\gamma_2 d \cdot \frac{1}{\Delta}\left[g_1(\alpha,\beta)\tilde{J}_x(\alpha)+g_2(\alpha,\beta)\tilde{J}_z(\alpha)\right] + \frac{\beta}{j\left(k_1^2-\beta^2\right)}\frac{1}{\Delta_g} \cdot\left[g_3(\alpha,\beta)\tilde{E}_x(\alpha)+g_4(\alpha,\beta)\tilde{E}_z(\alpha)\right] \quad (30)$$

$$A^{(h)}(\alpha) = \frac{\beta}{j\left(k_1^2-\beta^2\right)}\sinh\gamma_2 d \cdot \frac{1}{\Delta_g}\left[g_5(\alpha,\beta)\tilde{J}_x(\alpha) + g_6(\alpha,\beta)\tilde{J}_z(\alpha)\right] - \frac{\beta\omega\epsilon_1}{k_1^2-\beta^2}\frac{1}{\Delta_g} \cdot\left[g_7(\alpha,\beta)\tilde{E}_x(\alpha)+g_8(\alpha,\beta)\tilde{E}_z(\alpha)\right] \quad (31)$$

$$B^{(e)}(\alpha) = \frac{\beta\omega\mu_1}{k_2^2-\beta^2}\frac{1}{\Delta_g}\left[g_1(\alpha,\beta)\tilde{J}_x(\alpha)+g_2(\alpha,\beta)\tilde{J}_z(\alpha)\right] + j\frac{\beta}{k_2^2-\beta^2}\frac{1}{\Delta_g}\left[g_9(\alpha,\beta)\tilde{E}_x(\alpha)+g_{10}(\alpha,\beta)\tilde{E}_z(\alpha)\right] \quad (32)$$

$$B^{(h)}(\alpha) = \frac{\beta}{\omega\mu_2\gamma_2}\left[\tilde{E}_x(\alpha)+\frac{\alpha\beta}{k_2^2-\beta^2}\tilde{E}_z(\alpha)\right] \quad (33)$$

$$C^{(e)}(\alpha) = \frac{\beta}{j\left(k_2^2-\beta^2\right)}\tilde{E}_z(\alpha) \quad (34)$$

$$C^{(h)}(\alpha) = j\frac{\beta}{k_2^2-\beta^2}\frac{1}{\Delta_g}\left[g_{11}(\alpha,\beta)\tilde{J}_x(\alpha)-g_3(\alpha,\beta)\tilde{J}_z(\alpha)\right] - \frac{1}{\omega\mu_2\gamma_2}\frac{\beta}{k_2^2-\beta^2}\frac{1}{\Delta_g} \cdot\left[g_{12}(\alpha,\beta)\tilde{E}_x(\alpha)+g_{13}(\alpha,\beta)\tilde{E}_z(\alpha)\right] \quad (35)$$

$$D^{(e)}(\alpha) = \frac{\beta}{j\left(k_2^2-\beta^2\right)}\tilde{E}_z(\alpha) \quad (36)$$

$$D^{(h)}(\alpha) = \frac{\beta}{\omega\mu_1\gamma_1}\left[\tilde{E}_x(\alpha)+\frac{\alpha\beta}{k_2^2-\beta^2}\tilde{E}_z(\alpha)\right] \quad (37)$$

$$g_1(\alpha,\beta) = \alpha\beta\left[\mu_r\gamma_2\sinh\gamma_2 d + \gamma_1\cosh\nu_2 d\right] \quad (38)$$

$$g_2(\alpha,\beta) = \mu_r\gamma_2\left(k_1^2-\beta^2\right)\sinh\gamma_2 d + \gamma_1\left(k_2^2-\beta^2\right)\cosh\gamma_2 d \quad (39)$$

$$g_3(\alpha,\beta) = -\alpha\beta\left(k_1^2-k_2^2\right)\sinh\gamma_2 d \quad (40)$$

$$g_4(\alpha,\beta) = \left(k_1^2\alpha^2+k_2^2\beta^2-k_1^2k_2^2\right)\sinh\gamma_2 d + \epsilon_r\gamma_1\gamma_2 k_1^2\cosh\gamma_2 d \quad (41)$$

$$g_5(\alpha,\beta) = \mu_r\gamma_1\gamma_2 k_1^2\sinh\gamma_2 d + \left(k_1^2\alpha^2+k_2^2\beta^2-k_1^2k_2^2\right)\cosh\gamma_2 d \quad (42)$$

$$g_6(\alpha,\beta) = -\alpha\beta\left(k_1^2-k_2^2\right)\cosh\gamma_2 d \quad (43)$$

$$g_7(\alpha,\beta) = \gamma_1\left(k_2^2-\beta^2\right)\sinh\gamma_2 d + \epsilon_r\gamma_2\left(k_1^2-\beta^2\right)\cosh\gamma_2 d \quad (44)$$

$$g_8(\alpha,\beta) = \left[\gamma_1\sinh\gamma_2 d + \epsilon_r\gamma_2\cosh\gamma_2 d\right]\alpha\beta \quad (45)$$

$$g_9(\alpha,\beta) = \alpha\beta\left(k_1^2-k_2^2\right) \quad (46)$$

$$g_{10}(\alpha,\beta) = g(\alpha,\beta)+k_1^2\beta^2+k_2^2\alpha^2-k_1^2k_2^2 \quad (47)$$

$$g_{11}(\alpha,\beta) = \left(k_1^2\beta^2+k_2^2\alpha^2-k_1^2k_2^2\right)\sinh\gamma_2 d + \epsilon_r\gamma_1\gamma_2 k_1^2\cosh\gamma_2 d \quad (48)$$

$$g_{12}(\alpha,\beta) = \left(k_2^2-\beta^2\right)g(\alpha,\beta)+k_2^2\gamma_2^2\left(k_1^2-\beta^2\right) \quad (49)$$

$$g_{13}(\alpha,\beta) = \alpha\beta\left[g(\alpha,\beta)+k_2^2\gamma_2^2\right] \quad (50)$$

$$g(\alpha,\beta) = \left(k_1^2\gamma_2^2+k_2^2\gamma_1^2\right)\sinh^2\gamma_2 d + \gamma_1\gamma_2 k_1^2(\epsilon_r+\mu_r)\sinh\gamma_2 d\cosh\gamma_2 d \quad (51)$$

$$\Delta_g = g(\alpha,\beta)\cosh\gamma_2 d - \mu_r\gamma_1\gamma_2 k_1^2. \quad (52)$$

The exact expressions of Fourier transformed dyadic Green's functions are as follows:

$$G_{11}(\alpha,\beta) = j\omega\mu_1\sinh\gamma_2 d\cdot g_1(\alpha,\beta)/\Delta_g \quad (53)$$

$$G_{12}(\alpha,\beta) = j\omega\mu_1\sinh\gamma_2 d\cdot g_2(\alpha,\beta)/\Delta_g \quad (54)$$

$$G_{13}(\alpha,\beta) = g_3(\alpha,\beta)/\Delta_g \quad (55)$$

$$G_{14}(\alpha,\beta) = g_4(\alpha,\beta)/\Delta_g \quad (56)$$

$$G_{21}(\alpha,\beta) = j\omega\mu_1\sinh\gamma_2 d\cdot g_{14}(\alpha,\beta)/\Delta_g \quad (57)$$

$$G_{23}(\alpha,\beta) = g_{11}(\alpha,\beta)/\Delta_g \quad (58)$$

$$G_{33}(\alpha,\beta) = j\left[\gamma_2\cdot g_{15}(\alpha,\beta)\sinh\gamma_2 d\cosh\gamma_2 d + \gamma_1\cdot g_{16}(\alpha,\beta)\sinh^2\gamma_2 d + g_{17}(\alpha,\beta)\right]/\omega\mu_2\gamma_1\gamma_2\Delta_g \quad (59)$$

$$G_{34}(\alpha,\beta) = j\alpha\beta\left[\gamma_2\cdot g_{18}(\alpha,\beta)\sinh\gamma_2 d\cosh\gamma_2 d + \gamma_1\cdot g_{19}(\alpha,\beta)\sinh^2\gamma_2 d + g_{20}(\alpha,\beta)\right]/\omega\mu_2\gamma_1\gamma_2\Delta_g \quad (60)$$

$$G_{44}(\alpha,\beta) = -j\left[\gamma_2 \cdot g_{21}(\alpha,\beta)\sinh\gamma_2 d\cosh\gamma_2 d + \gamma_1 \cdot g_{22}(\alpha,\beta)\sinh^2\gamma_2 d + g_{23}(\alpha,\beta)\right]/\omega\mu_2\gamma_1\gamma_{2Dg} \quad (61)$$

$$g_{14}(\alpha,\beta) = \mu_r\gamma_2\left(k_1^2-\alpha^2\right)\sinh\gamma_2 d + \gamma_1\left(k_2^2-\alpha^2\right)\cosh\gamma_2 d$$

$$g_{15}(\alpha,\beta) = \mu_r\left(k_1^2-\beta^2\right)\left(k_1^2\gamma_2^2+k_2^2\gamma_1^2\right) + \gamma_1^2k_1^2\left(k_2^2-\beta^2\right)(\epsilon_r+\mu_r) \quad (62)(63)$$

$$g_{16}(\alpha,\beta) = \left(k_2^2-\beta^2\right)\left(k_1^2\gamma_2^2+k_2^2\gamma_1^2\right) + \mu_r\gamma_2^2k_1^2\left(k_1^2-\beta^2\right)(\epsilon_r+\mu_r) \quad (64)$$

$$g_{17}(\alpha,\beta) = 2\gamma_1\gamma_2^2k_2^2\left(k_1^2-\beta^2\right) \quad (65)$$

$$g_{18}(\alpha,\beta) = \mu_r\left(k_1^2\gamma_2^2+k_2^2\gamma_1^2\right)+\gamma_1^2k_1^2(\epsilon_r+\mu_r) \quad (66)$$

$$g_{19}(\alpha,\beta) = k_1^2\gamma_2^2+k_2^2\gamma_1^2+\mu_r\gamma_2^2k_1^2(\epsilon_r+\mu_r) \quad (67)$$

$$g_{20}(\alpha,\beta) = 2\gamma_1\gamma_2^2k_2^2 \quad (68)$$

$$g_{21}(\alpha,\beta) = \mu_r\left(k_1^2-\alpha^2\right)\left(k_1^2\gamma_2^2+k_2^2\gamma_1^2\right) + \gamma_1^2k_1^2\left(k_2^2-\alpha^2\right)(\epsilon_r+\mu_r) \quad (69)$$

$$g_{22}(\alpha,\beta) = \left(k_2^2-\alpha^2\right)\left(k_1^2\gamma_2^2+k_2^2\gamma_1^2\right) + \mu_r\gamma_2^2k_1^2\left(k_1^2-\alpha^2\right)(\epsilon_r+\mu_r) \quad (70)$$

$$g_{23}(\alpha,\beta) = 2\gamma_1\gamma_2^2k_2^2\left(k_1^2-\alpha^2\right). \quad (71)$$

The numerical expressions of $g(\alpha)$ for each region are as follows.

Region ①:

$$g_{①}(\alpha) = \left[\tilde{E}_{x1}(\alpha)\tilde{H}_{y1}^*(\alpha)-\tilde{E}_{y1}(\alpha)\tilde{H}_{x1}^*(\alpha)\right]/2\gamma_1 \quad (72)$$

$$\tilde{E}_{x1}(\alpha) = -j\alpha A^{(e)}(\alpha)-\omega\mu_1\gamma_1/\beta\cdot A^{(h)}(\alpha) \quad (73)$$

$$\tilde{E}_{y1}(\alpha) = -\gamma_1 A^{(e)}(\alpha)+j\alpha\omega\mu_1/\beta\cdot A^{(h)}(\alpha) \quad (74)$$

$$\tilde{H}_{x1}(\alpha) = \omega\epsilon_1\gamma_1/\beta\cdot A^{(e)}(\alpha)-j\alpha A^{(h)}(\alpha) \quad (75)$$

$$\tilde{H}_{y1}(\alpha) = j\alpha\omega\epsilon_1/\beta\cdot A^{(e)}(\alpha)-\gamma_1 A^{(h)}(\alpha). \quad (76)$$

Region ②:

$$g_{②}(\alpha) = \left[\tilde{E}_{x2s}(\alpha)\tilde{H}_{y2s}^*(\alpha)-\tilde{E}_{y2s}(\alpha)\tilde{H}_{x2s}^*(\alpha) + \tilde{E}_{x2c}(\alpha)\tilde{H}_{y2c}^*(\alpha)-\tilde{E}_{y2c}(\alpha)\tilde{H}_{x2c}^*(\alpha)\right]\cdot\sinh\gamma_2 d\cosh\gamma_2 d/2\gamma_2 + \left[-\tilde{E}_{x2s}(\alpha)\tilde{H}_{y2s}^*(\alpha)+\tilde{E}_{y2s}(\alpha)\tilde{H}_{x2s}^*(\alpha) + \tilde{E}_{x2s}(\alpha)\tilde{H}_{y2c}^*(\alpha)-\tilde{E}_{y2c}(\alpha)\tilde{H}_{x2c}^*(\alpha)\right]d/2 + \left[\tilde{E}_{x2s}(\alpha)\tilde{H}_{y2s}^*(\alpha)+\tilde{E}_{x2c}(\alpha)\tilde{H}_{y2c}^*(\alpha) - \tilde{E}_{y2s}(\alpha)\tilde{H}_{x2c}^*(\alpha) - \tilde{E}_{y2c}(\alpha)\tilde{H}_{x2s}^*(\alpha)\right]\sinh^2\gamma_2 d/2\gamma_2 \quad (77)$$

$$\tilde{E}_{x2s}(\alpha) = -j\alpha\beta^{(e)}(\alpha)+\omega\mu_2\gamma_2/\beta\cdot C^{(h)}(\alpha) \quad (78)$$

$$\tilde{E}_{y2s}(\alpha) = \gamma_2 C^{(e)}(\alpha)+j\alpha\omega\mu_2\gamma_2/\beta\cdot B^{(h)}(\alpha) \quad (79)$$

$$\tilde{H}_{x2s}(\alpha) = -\omega\epsilon_2\gamma_2/\beta\cdot C^{(e)}(\alpha)-j\alpha B^{(h)}(\alpha) \quad (80)$$

$$\tilde{H}_{y2s}(\alpha) = -j\alpha\omega\epsilon_2/\beta\cdot B^{(e)}(\alpha)+\gamma_2 C^{(h)}(\alpha) \quad (81)$$

$$\tilde{E}_{x2c}(\alpha) = -j\alpha C^{(e)}(\alpha)+\omega\mu_2\gamma_2/\beta\cdot B^{(h)}(\alpha) \quad (82)$$

$$\tilde{E}_{y2c}(\alpha) = \gamma_2 B^{(e)}(\alpha)+j\alpha\omega\epsilon_2/\beta\cdot C^{(h)}(\alpha) \quad (83)$$

$$\tilde{H}_{x2c}(\alpha) = -\omega\epsilon_2\gamma_2/\beta\cdot B^{(e)}(\alpha)-j\alpha C^{(h)}(\alpha) \quad (84)$$

$$\tilde{H}_{y2c}(\alpha) = -j\alpha\omega\epsilon_2/\beta\cdot C^{(e)}(\alpha)+\gamma_2 B^{(h)}(\alpha). \quad (85)$$

Region ③:

$$g_{③}(\alpha) = \left[\tilde{E}_{x3}(\alpha)\tilde{H}_{y3}^*(\alpha)-\tilde{E}_{y3}(\alpha)\tilde{H}_{x3}^*(\alpha)\right]/2\gamma_3 \quad (86)$$

$$\tilde{E}_{x3}(\alpha) = -j\alpha D^{(e)}(\alpha)+\omega\mu_3\gamma_3/\beta\cdot D^{(h)}(\alpha) \quad (87)$$

$$\tilde{E}_{y3}(\alpha) = \gamma_3 D^{(e)}(\alpha)+j\alpha\omega\mu_3/\beta\cdot D^{(h)}(\alpha) \quad (88)$$

$$\tilde{H}_{x3}(\alpha) = -\omega\epsilon_3\gamma_3/\beta\cdot D^{(e)}(\alpha)-j\alpha D^{(h)}(\alpha) \quad (89)$$

$$\tilde{H}_{y3}(\alpha) = -j\alpha\omega\epsilon_3/\beta\cdot D^{(e)}(\alpha)+\gamma_3 D^{(h)}(\alpha). \quad (90)$$

ACKNOWLEDGMENT

The authors would like to thank Dr. H. Yamamoto and Dr. K. Kohiyama for their valuable suggestions and guidance.

REFERENCES

[1] Special Issue on Microwave Integrated Circuits, *IEEE Trans. Microwave Theory Tech.*, vol. MTT-19, July 1971.

[2] Special Issue on Microwave and Millimeter-Wave Integrated Circuits, *IEEE Trans. Microwave Theory Tech*, vol. MTT-26, Oct. 1978.

[3] E. Hagihara, H. Ogawa, and M. Akaike, "A 26-GHz miniaturized MIC transmitter/receiver," *IEEE Trans. Microwave Theory Tech.*, vol. MTT-30, pp. 235–242, Mar. 1982.

[4] Y. Tokumitsu, M. Ishizaki, M. Iwakuni, and T. Saito, "50-GHz IC components using alumina substrates," *IEEE Trans. Microwave Theory Tech.*, vol. MTT-31, pp. 121–128, Feb. 1983.

[5] K. Chang, K. Louie, A. J. Grote, R. S. Tahim, M. J. Mlinar, G. M. Hayashibara, and C. Sun, "*V*-band low-noise integrated circuit receiver," *IEEE Trans. Microwave Theory Tech.*, vol. MTT-31, pp. 146–154, Feb. 1983.

[6] F. C. de Ronde, "A new class of microstrip directional coupler," in *Proc. IEEE Int. Microwave Symp.*, May 1970, pp. 184–186.

[7] M. Aikawa and H. Ogawa, "A new MIC magic-T using coupled slot lines," *IEEE Trans. Microwave Theory Tech.*, vol. MTT-28, pp. 523–528, June 1980.

[8] B. Schiek, "Hybrid branchline couplers—A useful new class of directional couplers," *IEEE Trans. Microwave Theory Tech.*, vol. MTT-22, pp. 864–869, Oct. 1974.

[9] R. K. Hoffmann and J. Siegl, "Microstrip-slot coupler design—Parts I and II," *IEEE Trans. Microwave Theory Tech.*, vol. MTT-30, pp. 1205–1216, Aug. 1982.

[10] H. Ogawa, M. Aikawa, and K. Morita, "*K*-band integrated double-balanced mixer," *IEEE Trans. Microwave Theory Tech.*, vol. MTT-28, pp. 180–185, Mar. 1980.

[11] L. E.. Dickens and D. W. Maki, "A new phased-type image enhanced mixer," in *IEEE MTT-S Int. Microwave Symp.*, May 1975, pp. 149–151.

[12] M. Aikawa and H. Ogawa, "2-GHz double-balanced PSK modulator using coplanar waveguide," in *IEEE Int. Solid State Circuits Conf.*, Feb. 1979, pp. 172–173.

[13] H. Ogawa, M. Aikawa, and M. Akaike, "Integrated balanced BPSK and QPSK modulators for the *Ka*-band," *IEEE Trans. Microwave Theory Tech.*, vol. MTT-30, pp. 227–234, Mar. 1982.
[14] K. J. Russell, "Microwave power combining techniques," *IEEE Trans. Microwave Theory Tech.*, vol. MTT-27, pp. 472–478, May 1979.
[15] E. Wilkinson, "An *N*-way hybrid power divider," *IRE Trans. Microwave Theory Tech.*, vol. MTT-8, pp. 116–118, Jan. 1960.
[16] L. I. Parad and R. L. Moynihan, "Split-tee power divider," *IEEE Trans. Microwave Theory Tech.*, vol. MTT-13, pp. 91–95, Jan. 1965.
[17] T. Matsumoto, "A coplanar power divider," *Trans. IECE Jap.*, vol. J60-B, pp. 525–526, July 1977.
[18] S. B. Cohn, "A class of broadband three-port TEM-mode hybrids," *IEEE Trans. Microwave Theory Tech.*, vol. MTT-16, pp. 110–116, Feb. 1968.
[19] J. Reed and G. J. Wheeler, "A method of analysis of symmetrical four-port networks," *IRE Trans. Microwave Theory Tech.*, vol. MTT-4, pp. 246–252, Oct. 1956.
[20] H. Ogawa and M. Aikawa, "Analysis of coupled microstrip-slot lines," *Trans. IECE Jap.*, vol. J62-B, pp. 396–403, Apr. 1979.
[21] T. Itoh and R. Mittra, "Dispersion characteristics of slot lines," *Electron. Lett.*, vol. 7, pp. 364–365, July 1971.
[22] T. Itoh and R. Mittra, "Spectral-domain approach for calculating the dispersion characteristics of microstrip lines," *IEEE Trans. Microwave Theory Tech.*, vol. MTT-21, pp. 496–499, July 1973.
[23] S. B. Cohn, "Slot line on a dielectric substrate," *IEEE Trans. Microwave Theory Tech.*, vol. MTT-17, pp. 768–778, Oct. 1969.
[24] J. B. Knorr and K. D. Kuchler, "Analysis of coupled slots and coplanar strips on dielectric substrate," *IEEE Trans. Microwave Theory Tech.*, vol. MTT-23, pp. 541–548, July 1975.
[25] H. Ogawa, T. Hirota, and M. Aikawa, "Coupled microstrip-slotline directional coupler," *Trans. IECE Jap.*, vol. J65-B, pp. 882–889, July 1982.
[26] S. Hopfer, "The design of ridged waveguide," *IRE Trans. Microwave Theory Tech.*, vol. MTT-3, pp. 20–29, Oct. 1955.
[27] F. C. de Ronde, *Neues aus der Technik*, VOGEL-VERLAG, 87 WURZBURG, W. GERMANY 1972-May-N°2-and.0.28.
[28] M. V. Schneider, B. Glance, and W. F. Bodtwen, "Microwave and mm wave hybrid integrated circuits for radio systems," *Bell System Tech. J.*, vol. 48, pp. 1703–1726, July/Aug. 1969.

✠

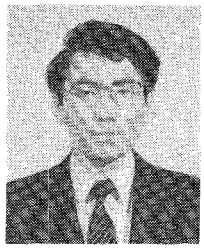

Hiroyo Ogawa (M'84) was born in Sapporo, Japan, in 1951. He received the B.S., M.S., and Ph.D. degrees in electrical engineering from the Hokkaido University, Sapporo, Japan, in 1974, 1976, and 1983, respectively.

He joined Yokosuka Electrical Communication Laboratories, Nippon Telegraph and Telephone Public Corporation, Yokosuka, in 1976, and has been engaged in the research of microwave integrated circuits. He is presently engaged in the research of millimeter-wave integrated circuits.

Dr. Ogawa is a member of the Institute of Electronics and Communication Engineering of Japan.

✠

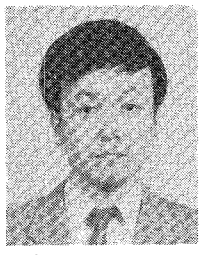

Tetsuo Hirota was born in Takaoka, Japan, in 1956. He received the B.S. and M.S. degrees in electronics from Kyoto University, Kyoto, Japan, in 1979 and 1981, respectively.

In 1981, he joined Yokosuka Electrical Communication Laboratory, Nippon Telegraph and Telephone Corporation, Yokosuka, Japan. He has been engaged in the research of microwave integrated circuits.

Mr. Hirota is a member of the Institute of Electronics and Communication Engineers of Japan.

✠

Masayoshi Aikawa (M'74) was born in Saga, Japan, on October 16, 1946. He received the B.S. and M.S. degrees in electrical engineering from the Kyushu University, Fukuoka, Japan, in 1969 and 1971, respectively.

He joined the Electrical Communication Laboratory, Nippon Telegraph and Telephone (NTT) Public Corporation, Tokyo, Japan, in 1971, and has since been engaged in researching and developing microwave integrated circuits for radio communication systems. He is now a senior staff engineer of the High Capacity Satellite Communication Section in Yokosuka Electrical Communication Laboratory, NTT, Yokosuka, Japan.

Mr. Aikawa is a member of the Institute of Electronics and Communication Engineers of Japan.